Implementation of the Boundary Integral Equation Neumann-to-Dirichlet map (BIE-NtD) method for the analysis of 1D-periodic diffraction gratings

Rodrigo Arrieta*
(Dated: May 17, 2024)

This report presents an implementation of the BIE-NtD method, as proposed by Wu and Lu (2009), for computing transmission and reflection coefficients of 1D-periodic diffraction gratings and photonic crystal (PhC) slabs. The approach totally bypasses the use of the problematic quasiperiodic Green's function, employing the free-space Green's function instead. We establish an analogy between this method and the Transfer Matrix Method (TMM) for planar isotropic layered media, identifying the BIE-NtD method as a direct generalization of the TMM for isotropic layered media with periodic interfaces. Furthermore, various examples demonstrating the application of the BIE-NtD method are showcased. We finally mention some potential suggestions to improve the speed and efficiency of the method.

I. PROBLEM FORMULATION

We consider diffraction gratings that are periodic in the $\hat{\mathbf{x}}$ direction, with period $L > 0$, and invariant in the $\hat{\mathbf{z}}$ direction. The grating comprises layers of isotropic and homogeneous materials, and it is contained in the region $0 \leq y \leq D$, as depicted in Fig. 1. The top ($y > D$) and bottom ($y < 0$) regions correspond also to infinite, homogeneous, and isotropic materials with permittivities $\epsilon^{(1)}$ and $\epsilon^{(2)}$, respectively. Assume that an incoming electromagnetic plane wave, propagating in the xy plane, impinges on the structure from the top domain $y > 0$, giving rise to a reflected wave in the top domain $y > 0$ and a transmitted wave in the bottom domain $y < 0$. Since the problem is z-invariant and every xy plane acts as a mirror symmetry plane, we can reduce our attention to only light polarized as transverse electric (TE or E_z polarization; the electric field only has a non-zero component in the z direction) or transverse magnetic (TM or H_z polarization; the magnetic field only has a non-zero component in the z direction). For simplicity, for the rest of this work we will focus our attention in the E_z polarized case. (The BIE-NtD method described here also works for H_z polarization; it requires, however, slight modifications.) Letting u be the total z-component of the electric field, we have that u satisfies the Helmholtz equation:

$$(\Delta + k_0^2 \epsilon(x,y))u(x,y) = 0, \tag{1}$$

where $k_0 = \omega/c$ is the free-space wavenumber, ω is the angular frequency, c is the speed of light in vacuum, and $\epsilon(x,y)$ is the permittivity at point (x,y). Furthermore, both u and its normal derivative $\partial u/\partial n$ are continuous across the interface between different materials.

Let the incoming plane wave coming from the top be

$$u^{(i)}(x,y) = e^{i(\alpha_0 x - \beta_0^{(1)} y)}, \qquad y > D, \tag{2}$$

where $\alpha_0 \in [-k_0\sqrt{\epsilon^{(1)}}, k_0\sqrt{\epsilon^{(1)}}]$ is the Bloch wavenumber and $\beta_0^{(1)} = \sqrt{k_0^2\epsilon^{(1)} - \alpha_0^2}$. The structure possesses discrete translational symmetry, with period L, in the x-direction, hence Bloch's theorem asserts that the Bloch wavenumber α_0 must be preserved up to multiples of $2\pi/L$. Let

$$\alpha_j = \alpha_0 + j\frac{2\pi}{L}, \qquad j \in \mathbb{Z}, \tag{3}$$

$$\beta_j^{(1,2)} = \sqrt{k_0^2\epsilon^{(1,2)} - \alpha_j^2}, \tag{4}$$

where the square root of a negative number is taken with a positive imaginary part. Then, the reflected and transmitted waves admit *outgoing Rayleigh-Bloch expansions* of the form

$$u^{(r)}(x,y) = \sum_{j=-\infty}^{\infty} R_j e^{i\left(\alpha_j x + \beta_j^{(1)}(y-D)\right)}, \quad y > D, \tag{5}$$

$$u^{(t)}(x,y) = \sum_{j=-\infty}^{\infty} T_j e^{i\left(\alpha_j x - \beta_j^{(2)} y\right)}, \quad y < 0, \tag{6}$$

where $R_j, T_j \in \mathbb{C}$ are (a priori unknown) reflection and transmission coefficients of the diffraction order $j \in \mathbb{Z}$, respectively. Given a diffraction grating, the goal is to compute these coefficients, possibly for a limited number of diffraction orders, say $j \in [-J, J]$. (The magnitude of the coefficients must decay as $|j| \to \infty$ for the Rayleigh-Bloch expansion to be absolutely convergent.) Note that only a finite number of diffraction orders possess a real $\beta_j^{(1)}$ and/or $\beta_j^{(2)}$. Diffraction orders with an imaginary $\beta_j^{(1)}$ and/or $\beta_j^{(2)}$ correspond to *evanescent waves*; they exponentially decay towards $y \to \infty$ and/or $y \to -\infty$, and carry no power.

Now, again by virtue of Bloch's theorem, we have that both u and $\partial u/\partial n$ are quasiperiodic with quasiperiod L, thus we can limit our analysis to the rectangular domain $\Sigma = \{(x,y) | \, 0 \leq x \leq L, \, 0 \leq y \leq D\}$ with *Bloch-periodic boundary conditions* on the lateral boundaries, given by

$$u(x = L, y) = \gamma u(x = 0, y), \tag{7}$$

$$\frac{\partial u}{\partial n}(x = L, y) = -\gamma \frac{\partial u}{\partial n}(x = 0, y), \tag{8}$$

* Mathematics Department, Massachusetts Institute of Technology, Cambridge, MA 02139, United States; rarrieta@mit.edu

where $\gamma = e^{i\alpha_0 L}$ and the minus sign of the last equation comes from the fact that the normal vectors at $x = 0$ and $x = L$ point towards opposite directions.

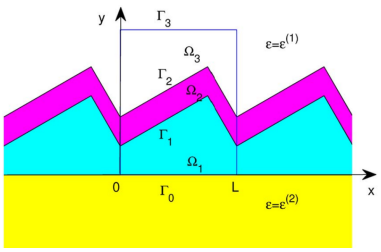

FIG. 1: A diffraction grating with multiple layers of different materials. Obtained from [1].

II. AN OVERVIEW OF EXISTING BIE METHODS FOR ANALYZING DIFFRACTION GRATINGS

Classical BIE formulations for scattering by periodic media rely on the quasi-periodic Green function [2]. As it is well-known, the standard representation of the quasi-periodic Green function entails evaluating an infinite series that converge slowly and cease to exist at Wood anomalies. Various methods exist to accelerate the convergence of this series, the most notable being Ewald's method [2]. As a simple alternative, in [3, 4] the authors utilize a smooth windowed sum approximation of the infinite series, achieving superalgebraically fast convergence away from Wood anomalies.

In another approach developed in [5, 6], the quasiperiodic problem is reformulated into a second-kind indirect BIE formulation involving the free-space Green's function and integrating along the infinite boundaries of the unit-cell domain. By exploiting the exponential decay of boundary integrands in spectral form, the resulting BIE system is simplified into a bounded hybrid spatial-spectral computational domain, enabling the application of standard Nyström discretizations for numerical solution. Despite not utilizing the quasi-periodic Green function, this approach requires handling cumbersome Sommerfeld-type integrals, which are particularly challenging in the presence of Wood anomalies, where contour deformations and residue contributions are necessary.

A recent contribution [7] follows a similar approach as [5, 6]: a second-kind indirect BIE formulation involving the free-space Green's function is obtained, which requires integrating along the infinite boundaries of the unit-cell domain. However, the infinite boundaries are no longer handled in in the spectral domain, but directly in the spatial domain by relying on the Windowed Green Function (WGF) method [8] for their computation.

This section requires expansion.

III. THE BOUNDARY INTEGRAL EQUATION NEUMANN-TO-DIRICHLET MAP (BIE-NTD) METHOD

The BIE-NtD method [9] is a BIE method for the computation of the reflection and transmission coefficients (Eqs. (5) and (6)) which relies in (1) the discretization of the boundaries of the retangular domain Σ and the material boundaries therein, and (2) the employment of integral operators involving only the free-space Green's function, totally bypassing the use of the quasiperiodic Green's function. The methodology works in a similar fashion as the Transfer Matrix Method (TMM) [10, 11], which is often employed in the analysis of planar layered and isotropic media: "Transfer Matrices" are constructed for each homogeneous region Ω_j (see Fig. 1), which relate the (discretized) values of u and $\partial u/\partial n$ between the boundaries Γ_j and Γ_{j+1}. Then, these Transfer Matrices are concatenated to relate u and $\partial u/\partial n$ of the bottom and top boundaries (Γ_0 and Γ_3 in Fig. 1). With this, the incident wave Eq. (2) and the Rayleigh-Bloch expansions of Eqs. (5) and (6) can be related, which allows to solve for the reflection and transmission coefficients R_j and T_j. The Transfer Matrices are effectively constructed by solving a boundary integral equation and obtaining the NtD map of each homogeneous domain Ω_j.

In this section, instead of presenting a full and technical description of the BIE-NtD method, which can be found in Wu and Lu's paper [9], we will present a comparison between the TMM and the BIE-NtD method. In a sense, the BIE-NtD method can be understood as a generalization of the TMM for isotropic layered media with periodic and non-necessarily-planar interfaces.

Let us start by describing the TMM, employed to analyze reflection and transmission by isotropic layered media. Referring to Fig. 2, consider the homogeneous region Ω_j between the planar interfaces Γ_j and Γ_{j+1}, with thickness h_j and permittivity ϵ_j. In the TMM, the values of the E_z and H_x fields between the interfaces Γ_j and Γ_{j+1} are related by a Transfer Matrix. Since the phase of the wave in the x-direction is known and the same for both interfaces (due to continuous translational symmetry in the x-direction), then only one discretization point is necessary in each interface to describe the electromagnetic field along the whole interface (the discretization point is marked in purple in Fig. 2; assume that the x-component is the same for both interfaces, say $x = 0$). Then, we can write

$$\begin{pmatrix} E_z(y+h_j) \\ H_x(y+h_j) \end{pmatrix} = M_j \begin{pmatrix} E_z(y) \\ H_x(y) \end{pmatrix}, \tag{9}$$

where M_j is the Transfer Matrix of region Ω_j. The simplicity of the problem allows us to write M_j in closed form as

$$M_j = \begin{pmatrix} \cos(k_j h_j) & iZ_j \sin(k_j h_j) \\ \frac{i}{Z_j}\sin(k_j h_j) & \cos(k_j h_j) \end{pmatrix}, \tag{10}$$

where k_j is the wavenumber and Z_j is the characteristic impedance of region Ω_j, which depends on ϵ_j and the angle of incidence.

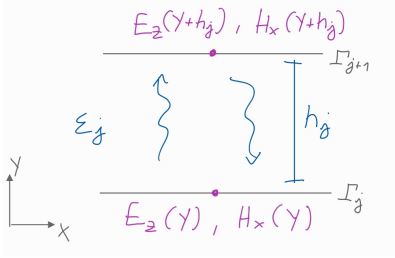

FIG. 2: An homogeneous region of thickness h_j and permittivity ϵ_j, delimited by the two planar interfaces Γ_j and Γ_{j+1}. The purple point depicts discretization points at the top and bottom interface.

Now, consider a stack of layered regions with total thickness D, as shown in Fig. 3. Given an incident wave from the top, we wish to compute the reflected and transmitted wave generated by this structure. Analogous to what was shown in Section I, we can write the fields in the top and bottom regions as

$$E_z^{(\text{top})}(x,y) = e^{i(\alpha_0 x - \beta_0^{(1)} y)} + Re^{i(\alpha_0 x + \beta_0^{(1)}(y-D))}, \quad (11)$$

$$H_x^{(\text{top})}(x,y) = -\frac{1}{Z_{\text{top}}} e^{i(\alpha_0 x - \beta_0^{(1)} y)} + \frac{1}{Z_{\text{top}}} Re^{i(\alpha_0 x + \beta_0^{(1)}(y-D))}, \quad (12)$$

for $y > D$, and

$$E_z^{(\text{bottom})}(x,y) = Te^{i(\alpha_0 x - \beta_0^{(2)} y)}, \quad (13)$$

$$H_x^{(\text{bottom})}(x,y) = -\frac{1}{Z_{\text{bottom}}} Te^{i(\alpha_0 x - \beta_0^{(2)} y)}, \quad (14)$$

for $y < 0$, where R and T are the reflection and transmission coefficients, respectively. It is convenient, as we shall later see for the BIE-NtD method, to define two Fourier multiplier operators, $\mathcal{B}_{\text{TMM}}^{(\text{top})}$ and $\mathcal{B}_{\text{TMM}}^{(\text{bottom})}$, defined by their action on the Fourier basis (or, more precisely, Fourier-Bloch basis):

$$i\mathcal{B}_{\text{TMM}}^{(s)} e^{i\alpha_j x} = \frac{1}{Z_s} e^{i\alpha_j x}, \quad (15)$$

for $j \in \mathbb{Z}$ and $s =$ top or $s =$ bottom. Hence, we can employ these operators to express the magnetic field in terms of the electric field:

$$H_x(x,D) = i\mathcal{B}_{\text{TMM}}^{(\text{top})} E_z(x,D) - \frac{2}{Z_{\text{top}}} e^{i\alpha_0 x}, \quad (16)$$

$$H_x(x,0) = -i\mathcal{B}_{\text{TMM}}^{(\text{bottom})} E_z(x,0), \quad (17)$$

for all $x \in \mathbb{R}$. Therefore, following the TMM formalism, we can relate the fields at the top and bottom interface as

$$\begin{pmatrix} E_z(x,D) \\ H_x(x,D) \end{pmatrix} = M \begin{pmatrix} E_z(x,0) \\ H_x(x,0), \end{pmatrix}, \quad (18)$$

where $M = M_{N-1}M_{N-2}\dots M_1 M_0$ is the total Transfer Matrix, obtained by multiplying the Transfer Matrices of each layer. Equivalently, we can write

$$\begin{pmatrix} E_z(x,D) \\ i\mathcal{B}_{\text{TMM}}^{(\text{top})} E_z(x,D) - \frac{2}{Z_{\text{top}}} e^{i\alpha_0 x} \end{pmatrix} = M \begin{pmatrix} E_z(x,0) \\ i\mathcal{B}_{\text{TMM}}^{(\text{bottom})} E_z(x,0), \end{pmatrix}, \quad (19)$$

which, for each x (although for this case is sufficient to consider $x = 0$ only,) is a linear system of two equations involving two unknowns: $E_z(x,D)$ and $E_z(x,0)$. Once the unknowns are solved, the reflection and transmission coefficients, R and T, can be computed from Eqs. (11) and (13), respectively.

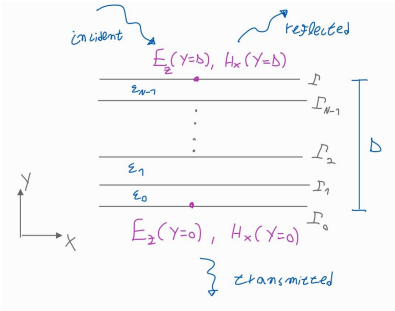

FIG. 3: A stack of layered regions with planar interfaces and total thickness D.

The BIE-NtD method, on the other hand, works in exactly the same manner as the TMM; it is, however, much more general, since it allows to handle interfaces that are not necessarily planar, but periodic.

Consider a region Ω_j, with permittivity ϵ_j, which is delimited by the periodic interfaces Γ_j and Γ_{j+1}, both with period L, as depicted in Fig. 4. The solutions u and $\partial u/\partial n$ at the interfaces can no longer be represented by a single discretization point; in general, they are quasiperiodic functions, with quasiperiod L, so an alternative to represent them is to discretize using many points, in only one quasiperiod, along both interfaces Γ_j and Γ_{j+1}, as shown with the purple dots in Fig. 4. Note that it is not necessary that the x-components of the points on the top and bottom interfaces to coincide, or to have the same number of points; moreover, the spacing between points does not have to be uniform. This construction yields four vectors of unknowns, namely $\boldsymbol{u}_{\Gamma_j}$, $\partial_n \boldsymbol{u}_{\Gamma_j}$, $\boldsymbol{u}_{\Gamma_{j+1}}$, and $\partial_n \boldsymbol{u}_{\Gamma_{j+1}}$. Now, following the same logic as in the TMM, let us assume that a Transfer Matrix M_j relates the top and bottom unknowns as

$$\begin{pmatrix} \boldsymbol{u}_{\Gamma_{j+1}} \\ \partial_n \boldsymbol{u}_{\Gamma_{j+1}} \end{pmatrix} = M_j \begin{pmatrix} \boldsymbol{u}_{\Gamma_j} \\ \partial_n \boldsymbol{u}_{\Gamma_j} \end{pmatrix}. \quad (20)$$

For the moment we will assume that M_j exists and it is given. The procedure for its construction will be provided later in Section III A.

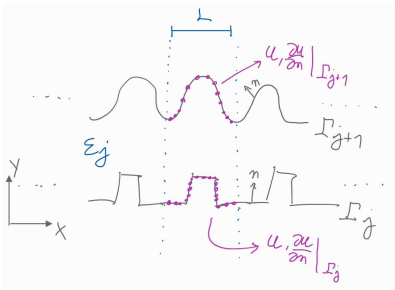

FIG. 4: An homogeneous region with permittivity ϵ_j, delimited by the two periodic interfaces Γ_j and Γ_{j+1}, with period L. The purple points depict discretization points of u and $\partial_n u$ at the top and bottom interface.

Given the Transfer Matrices of all regions, we can consider the diffraction problem (Section I) of a multilayer grating with periodic interfaces, with period L, as shown in Fig. 5. The unknowns of the top and bottom interface can be related as

$$\begin{pmatrix} \boldsymbol{u}_{\Gamma_N} \\ \partial_n \boldsymbol{u}_{\Gamma_N} \end{pmatrix} = M \begin{pmatrix} \boldsymbol{u}_{\Gamma_0} \\ \partial_n \boldsymbol{u}_{\Gamma_0}, \end{pmatrix}, \tag{21}$$

where $M = M_{N-1} M_{N-2} \dots M_1 M_0$ is the total Transfer Matrix, obtained by multiplying the Transfer Matrices of each layer. It is convenient to introduce two Fourier multiplier operators, $\mathcal{B}^{(1)}$ and $\mathcal{B}^{(2)}$, defined by their action on the Fourier basis:

$$i\mathcal{B}^{(s)} e^{i\alpha_j x} = i\beta_j^{(s)} e^{i\alpha_j x}, \tag{22}$$

for $j \in \mathbb{Z}$ and $s = 1, 2$. In practice, the $i\mathcal{B}^{(s)}$ operators are approximated by matrices; their construction is outlined in Section III C. Hence, using the Rayleigh-Bloch expansions of the top and bottom domains (Eqs. (5) and (6)) and the fact that the interfaces Γ_N and Γ_0 are flat, and thus $\partial_n = \partial_y$, we can employ $\mathcal{B}^{(1)}$ and $\mathcal{B}^{(2)}$ operators to express $\partial_n \boldsymbol{u}$ in terms of $\boldsymbol{u}$:

$$\partial_n \boldsymbol{u}_{\Gamma_N}(x) = i\mathcal{B}^{(1)} \boldsymbol{u}_{\Gamma_N}(x) - 2i\beta_0 e^{i\alpha_0 x}, \quad x \in \Gamma_N, \tag{23}$$

$$\partial_n \boldsymbol{u}_{\Gamma_0}(x) = -i\mathcal{B}^{(2)} \boldsymbol{u}_{\Gamma_0}(x), \qquad x \in \Gamma_0. \tag{24}$$

Thus, Eq. (21) can be rewritten as a linear system for two unknowns $\boldsymbol{u}_{\Gamma_N}$ and $\boldsymbol{u}_{\Gamma_0}$:

$$A \begin{pmatrix} \boldsymbol{u}_{\Gamma_N} \\ \boldsymbol{u}_{\Gamma_0} \end{pmatrix} = \begin{pmatrix} \boldsymbol{0} \\ \boldsymbol{b} \end{pmatrix}, \tag{25}$$

where the matrix A is given by, in block matrix form:

$$A = \begin{pmatrix} I & -M_{11} + M_{12} i\mathcal{B}^{(2)} \\ i\mathcal{B}^{(1)} & -M_{21} + M_{22} i\mathcal{B}^{(2)} \end{pmatrix}, \tag{26}$$

where the submatrices M_{ij} are conformable subblocks of the matrix M:

$$M = \begin{pmatrix} M_{11} & M_{12} \\ M_{21} & M_{22} \end{pmatrix}, \tag{27}$$

and the vector $\boldsymbol{b}$ is given by $\boldsymbol{b} = (2i\beta_0 e^{i\alpha_0 x} \text{ for } x \in \Gamma_N)^\top$. Solving Eq. (25) yields $\boldsymbol{u}_{\Gamma_N}$ and $\boldsymbol{u}_{\Gamma_0}$. To obtain the reflection and transmission coefficients, we notice that the reflected field at Γ_N, given by $\boldsymbol{u}^{(r)} = \boldsymbol{u}_{\Gamma_N} - \boldsymbol{u}^{(i)}_{\Gamma_N}$, and the transmitted field at Γ_0, which is $\boldsymbol{u}^{(t)} = \boldsymbol{u}_{\Gamma_0}$, can be written using Eqs. (5) and (6) as

$$u^{(r)}(x) = \sum_{j=-\infty}^{\infty} R_j e^{i\alpha_j x}, \qquad x \in \Gamma_N, \tag{28}$$

$$u^{(t)}(x) = \sum_{j=-\infty}^{\infty} T_j e^{i\alpha_j x}, \qquad x \in \Gamma_0. \tag{29}$$

Thus, the reflection ans transmission coefficients can be obtained by inverting these Fourier-Bloch series:

$$R_j = \frac{1}{L} \int_0^L u^{(r)}(x) e^{-i\alpha_j x} \, \mathrm{d}x, \tag{30}$$

$$T_j = \frac{1}{L} \int_0^L u^{(t)}(x) e^{-i\alpha_j x} \, \mathrm{d}x, \tag{31}$$

$$\tag{32}$$

for $j \in \mathbb{Z}$, which can be computed numerically by employing the discretizations $\boldsymbol{u}^{(r)}$ and $\boldsymbol{u}^{(t)}$.

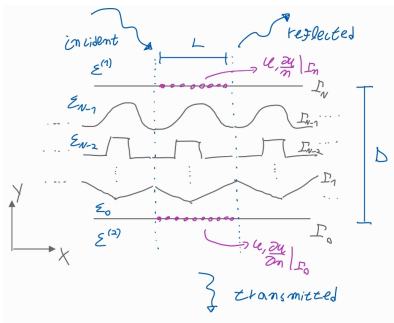

FIG. 5: A stack of layered regions with periodic interfaces, with period L, and total thickness D.

A. Construction of the Transfer Matrix via the NtD map

A key component of the BIE-NtD method is the construction of the Transfer Matrices M_j, which relate the values of u and $\partial_n u$ between two adjacent interfaces, as shown in Eq. (20), and, as the name of the method implies, their construction involves solving a Boundary Integral Equation and computing the Neumann-to-Dirichlet map of each homogeneous region.

In a closed region Ω_j, with boundary $\partial\Omega_j$ and normal vector $\boldsymbol{n}$ pointing outwards, the Neumann-to-Dirichlet map is an operator that relates the values of u and $\partial_n u$ on the boundary $\partial\Omega_j$, a relation that can be written as

$$\boldsymbol{u}_{\partial\Omega_j} = \mathcal{V}_j \left(\partial_n \boldsymbol{u}_{\partial\Omega_j}\right), \tag{33}$$

where $\mathcal{V}_j$ is the NtD map of region Ω_j. In practice, $\mathcal{V}_j$ is approximated by a matrix that relates the point values of u and $\partial_n u$ on the boundary; its construction is outlined in Section III B.

Consider, for instance, a closed domain Ω_j, with permittivity ϵ_j, delimited by the interfaces Γ_j and Γ_{j+1}, and by vertical boundaries at $x = 0$ and $x = L$, as illustrated in Fig. 6. Denoting $\boldsymbol{v}_j = \boldsymbol{u}|_{x=0}$, $\boldsymbol{w}_j = \boldsymbol{u}|_{x=L}$, $\boldsymbol{u}_j = \boldsymbol{u}|_{\Gamma_j}$, and $\boldsymbol{u}_{j+1} = \boldsymbol{u}|_{\Gamma_{j+1}}$, we can rewrite Eq. (33) by partitioning $\mathcal{V}_j$ in blocks:

$$\begin{pmatrix} \boldsymbol{u}_{j-1} \\ \boldsymbol{v}_j \\ \boldsymbol{w}_j \\ \boldsymbol{u}_j \end{pmatrix} = \begin{pmatrix} \mathcal{V}_{11} & \mathcal{V}_{12} & \mathcal{V}_{13} & \mathcal{V}_{14} \\ \mathcal{V}_{21} & \mathcal{V}_{22} & \mathcal{V}_{23} & \mathcal{V}_{24} \\ \mathcal{V}_{31} & \mathcal{V}_{32} & \mathcal{V}_{33} & \mathcal{V}_{34} \\ \mathcal{V}_{41} & \mathcal{V}_{42} & \mathcal{V}_{43} & \mathcal{V}_{44} \end{pmatrix} \begin{pmatrix} \partial_n \boldsymbol{u}_{j-1} \\ \partial_n \boldsymbol{v}_j \\ \partial_n \boldsymbol{w}_j \\ \partial_n \boldsymbol{u}_j \end{pmatrix}. \tag{34}$$

Our goal is to relate $(\boldsymbol{u}_{j+1}, \partial_n \boldsymbol{u}_{j+1})$ with $(\boldsymbol{u}_j, \partial_n \boldsymbol{u}_j)$ using a Transfer Matrix M_j. If $(\boldsymbol{u}_j, \partial_n \boldsymbol{u}_j)$ are given, then Eq. (34) is a linear system of $4r$ equations, where r is the length of each vector, for $6r$ unknowns, which are $\boldsymbol{u}_{j+1}, \partial_n \boldsymbol{u}_{j+1}, \boldsymbol{v}_j, \partial_n \boldsymbol{v}_j, \boldsymbol{w}_j$, and $\partial_n \boldsymbol{w}_j$. (For simplicity we have assumed that each vector has the same length r; however, this argument still works if we only demand that the lateral unknowns $\boldsymbol{v}_j, \partial_n \boldsymbol{v}_j, \boldsymbol{w}_j, \partial_n \boldsymbol{w}_j$ have the same length.) Notice that the Bloch-periodic boundary conditions of Eqs. (7) and (8) provide us with additional $2r$ equations, namely

$$\boldsymbol{w}_j = \gamma \boldsymbol{v}_j, \tag{35}$$

$$\partial_n \boldsymbol{w}_j = -\gamma \partial_n \boldsymbol{v}_j, \tag{36}$$

and thus we have a square system for our $6r$ unknowns. To obtain the Transfer Matrix M_j, we can formally express the lateral unknowns in terms of $\boldsymbol{u}_{j+1}$ and $\partial_n \boldsymbol{u}_{j+1}$, and then eliminate them from the system of equations (this is done via *Schur complements*), after which we finally obtain a system of equations that relates $(\boldsymbol{u}_{j+1}, \partial_n \boldsymbol{u}_{j+1})$ with $(\boldsymbol{u}_j, \partial_n \boldsymbol{u}_j)$, this is

$$\begin{pmatrix} \boldsymbol{u}_{j+1} \\ \partial_n \boldsymbol{u}_{j+1} \end{pmatrix} = M_j \begin{pmatrix} \boldsymbol{u}_j \\ \partial_n \boldsymbol{u}_j \end{pmatrix}, \tag{37}$$

where the Transfer Matrix M_j was obtained by eliminating the lateral variables from Eqs. (34) to (36).

B. Construction of the NtD map

A way of constructing the NtD map for a closed region is to rely on *the Green's representation formula* [12], also known as *the Principle of Equivalence*, which asserts that a solution u of the Hemlholtz equation in a closed domain

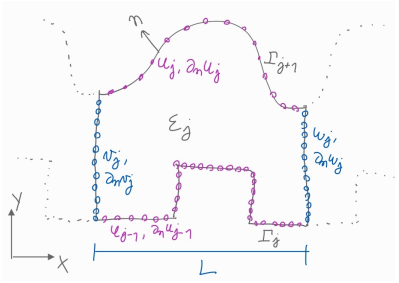

FIG. 6: A closed region with permittivity ϵ_j, delimited by the two periodic interfaces Γ_j and Γ_{j+1}, with period L, and vertical walls at $x = 0$ and $x = L$. The purple and blue points depict discretization points of u and $\partial_n u$ at the boundary of the domain.

Ω can be express solely in terms of the values of u and $\partial_n u$ on the boundary $\Gamma = \partial\Omega$. For a closed domain Ω with wavenumber k, such as the one shown in Fig. 6 (for simplicity let us drop the subscripts j,) we have that

$$u(x) = \mathcal{S}[\partial_n u](x) - \mathcal{D}[u](x), \qquad x \in \Omega, \tag{38}$$

where

$$\mathcal{S}[\phi](x) = \oint_\Gamma G(x,y)\phi(y)\,\mathrm{d}s_y, \tag{39}$$

$$\mathcal{D}[\phi](x) = \oint_\Gamma \frac{\partial G(x,y)}{\partial_{n_y}}\phi(y)\,\mathrm{d}s_y, \quad x \in \Omega, \tag{40}$$

are the *single-layer* and *double-layer* potentials, $G(x,y) = \frac{i}{4}H_0^{(1)}(k\,|x-y|)$ is the *free-space Green's function* of the Helmholtz equation in two dimensions, and $H_0^{(1)}$ is the Hankel function of the first kind of order zero. By taking the limit $x \to \Gamma$, and taking into account the well-known jump of the double-layer potential [12], we have that

$$\frac{u(x)}{2} + \mathcal{D}[u](x) = \mathcal{S}[\partial_n u](x), \qquad x \in \Gamma, \tag{41}$$

or in its discretized form,

$$\left(\frac{I}{2} + \mathrm{D}\right)\boldsymbol{u}_\Gamma = \mathrm{S}(\partial_n \boldsymbol{u}_{\partial\Omega}), \tag{42}$$

which is a Fredholm integral equation of the second kind for $\boldsymbol{u}_\Gamma$. Then, we have that

$$\boldsymbol{u}_\Gamma = \left(\frac{I}{2} + \mathrm{D}\right)^{-1} \mathrm{S}(\partial_n \boldsymbol{u}_\Gamma), \tag{43}$$

and thus the Neumann-to-Dirichlet map is given by $\mathcal{V} = \left(\frac{I}{2} + \mathrm{D}\right)^{-1}\mathrm{S}$. The inverse of the $\left(\frac{I}{2} + \mathcal{D}\right)$ operator always exists, except for a discrete and infinite set of k^2 wavenumbers that correspond to the Neumann eigenvalues of the domain Ω [12].

C. Construction of the $i\mathcal{B}^{(1)}$ and $i\mathcal{B}^{(2)}$ operators

Consider a quasiperiodic function f with quasiperiod L, which can be written as a Fourier-Bloch series:

$$f(x) = \sum_{j=-\infty}^{\infty} \hat{f}_j e^{i\alpha_j x}, \quad x \in [0, L], \tag{44}$$

where

$$\hat{f}_j = \frac{1}{L}\int_0^L f(x) e^{-i\alpha_j x}\,\mathrm{d}x, \quad j \in \mathbb{Z}. \tag{45}$$

By definition, we have that (Eq. (22))

$$(i\mathcal{B}^{(s)} f)(x) = \sum_{j=-\infty}^{\infty} i\beta^{(s)} \hat{f}_j e^{i\alpha_j x}, \quad x \in [0, L], \tag{46}$$

for $s = 1, 2$. Therefore,

$$(i\mathcal{B}^{(s)} f)(x) = \sum_{j=-\infty}^{\infty} i\beta^{(s)} \left(\frac{1}{L}\int_0^L f(t) e^{-i\alpha_j t}\,\mathrm{d}t\right) e^{i\alpha_j x} \tag{47}$$

for $x \in [0, L]$, which can be numerically computed using the point values of f along $[0, L]$.

D. Regions with inclusions

The BIE-NtD method is also compatible with regions with inclusions; the only difference is that the NtD map $\mathcal{V}$ must be slightly modified. Consider the region with inclusion shown in Fig. 7, which consists in an interior region, with wavenumber k_B and boundary Γ_B, embedded in an exterior region with wavenumber k_A and boundary Γ_A. Denote by S_{AB} the matrix that maps a density ϕ_B, defined on Γ_B, onto Γ_A using the single-layer operator, and similarly for S_{BA} and the double-layer operator (all operators use the same k_A wavenumber). Then, similarly as Eq. (42), we have

$$\frac{\boldsymbol{u}_A}{2} = \mathrm{S}_{AA}(\partial_n \boldsymbol{u}_A) - \mathrm{D}_{AA}\boldsymbol{u}_A - \mathrm{S}_{AB}(\partial_n \boldsymbol{u}_B) - \mathrm{D}_{AB}\boldsymbol{u}_B, \tag{48}$$

$$\frac{\boldsymbol{u}_B}{2} = \mathrm{S}_{BA}(\partial_n \boldsymbol{u}_A) - \mathrm{D}_{BA}\boldsymbol{u}_A - \mathrm{S}_{BB}(\partial_n \boldsymbol{u}_B) - \mathrm{D}_{BB}\boldsymbol{u}_B, \tag{49}$$

where $\boldsymbol{u}_A$ denotes the values of u on Γ_A, and similarly for $\boldsymbol{u}_B$. Using the NtD map $\mathcal{V}_B$ of the interior region, we have that $\boldsymbol{u}_B = \mathcal{V}_B(\partial_n \boldsymbol{u}_B)$, and thus, after some tedious algebra, we can eliminate $\boldsymbol{u}_B$ and $\partial_n \boldsymbol{u}_B$ from the previous equations to yield a modified NtD map $\tilde{\mathcal{V}}$ such that

$$u_A = \tilde{\mathcal{V}}_A(\partial_n \boldsymbol{u}_A). \tag{50}$$

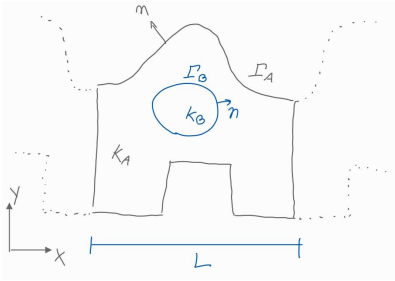

FIG. 7: Region with inclusion. An interior region, with wavenumber k_B and boundary Γ_B, is embedded in an exterior region with wavenumber k_A and boundary Γ_A.

IV. NUMERICAL EXAMPLES

The BIE-NtD method was programmed in the Julia Programming Language. Non-singular integral operators were discretized using the trapezoidal rule, whereas singular integral operators were discretized using the spectrally-accurate Nyström method by Martensen and Kussmaul [13, 14], as described by Colton and Kress [15]. As suggested by the latter authors, and by Wu and Lu [9], we employed a graded mesh to resolve possible singularities of the integral densities at the domains' corners. The code is available at `https://github.com/Riarrieta/DiffGrating1D`.

A. First example

For our first numerical example, which serves as a validation of our code, we consider the two sinusoidal gratings of Fig. 8. The first one comprises a sinusoidal profile which separates air and a different homogeneous medium. For a grove depth of $d = L$, a wavelength of $\lambda = L/1.7$ and $\alpha_0 = \pi/\lambda$, the computed reflection and transmission efficiencies are shown in Table I, where we also compare our values with the ones obtained by Li [16], employing the C method, and by Wu and Lu [9]. Using a similar discretization as Wu an Lu, it is observed that our results match their results, at least up to six decimal places. For the second grating with parameters $d_1 = 0.1L/\pi$, $d_2 = 0.4L/\pi$, which has a limited extent in the y-direction and separates two regions of air, we considered two different incident plane waves: one with $\lambda = L/1.9$ and angle of incidence of $15.2575°$, measured with respect to the y-axis, and another with $\lambda = L$ and angle of incidence of $30°$. For each case we compared our computed reflection and transmission efficiencies with results obtained by Magath et al. [17] and by Wu and Lu [9]; this is shown in Table II. It is observed that our results, obtained with a similar discretization as the one used by Wu and Lu, match the results of the other authors, up to five decimal places.

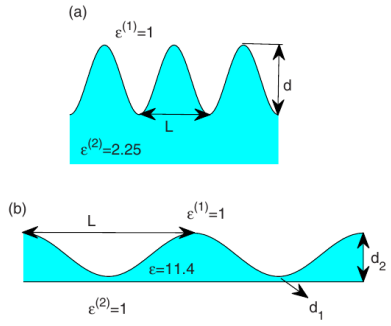

FIG. 8: Two sinusoidal diffraction gratings. In (a) the sinusoidal profile divides air and an homogeneous region. In (b) the grating has finite thickness and divides two regions of air.

TABLE I: First example. Reflection and transmission efficiencies for various diffraction orders, for grating (a) of Fig. 8.

Order	Li [16]	Wu and Lu [9]	This work
R, -1	0.7815037×10^{-3}	$0.78150378 \times 10^{-3}$	$0.78150394 \times 10^{-3}$
R, 0	0.2103160×10^{-2}	$0.21031606 \times 10^{-2}$	$0.21031607 \times 10^{-2}$
T, -1	0.4947933	0.49479330	0.49479329
T, 0	0.2086662	0.20866625	0.20866625
T, 1	0.1183058	0.11830582	0.11830581

TABLE II: Second example. Reflection and transmission efficiencies for various diffraction orders, for grating (b) of Fig. 8.

L/λ	Order	Magath et al. [17]	Wu and Lu [9]	This work
1.9	R, -2	0.1632	0.16337787	0.16337768
1.9	R, -1	0.5312	0.53111858	0.53111788
1.9	R, 0	0.0650	0.06506795	0.06506801
1.9	R, 1	0.1538	0.15381827	0.15381866
1	R, -1	0.0401	0.03989897	0.03989898
1	R, 0	0.4777	0.47833249	0.47833248
1	T, -1	0.2794	0.27947198	0.27947200
1	T, 0	0.2029	0.20229650	0.20229652

B. Second example

We consider the second grating of Fig. 8, but with a variable sinusoidal amplitude, given by $A \times 0.4L/\pi$ (originally $A = 1$.) For $A = 0.5$ we plotted the transmission efficiency of the zeroth-order as a function of angular frequency ω and Bloch wavevector α_0 (k_x in the figures), which is shown in Fig. 9. We observe clear zig-zagging dips in the transmittance spectrum, which correspond to guided modes of the structure that become leaky as the periodic sinusoidal profile is introduced. These leaky modes give rise to a characteristic Fano resonance lineshape [18], which can be observed in Fig. 10, where the transmission efficiency as a function of angular frequency is plotted, for $\alpha_0 L/2\pi = 0.245$. Here, a strange kink around $\omega L/2\pi c = 0.75$ can be observed, which can also be noted at the top left corner of Fig. 9b; its origin is unknown.

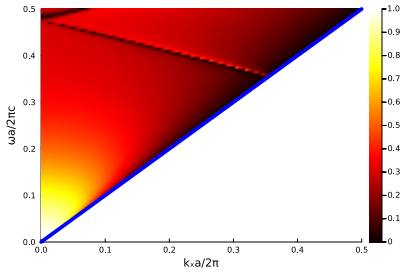

(a) Transmittance for normalized angular frequency between 0 and 0.5. The light line is shown in blue.

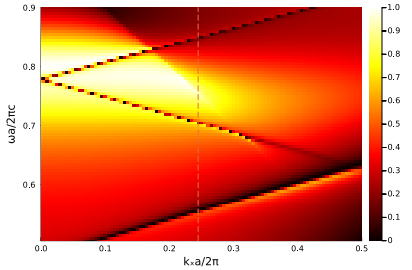

(b) Transmittance for normalized angular frequency between 0.5 and 0.9. We mark the normalized Bloch wavenumber 0.25 with a dashed line. The transmittance for this value is later plotted in Fig. 10.

FIG. 9: Second example. Transmittance of the zeroth-order diffraction as a function of angular frequency and Bloch wavenumber.

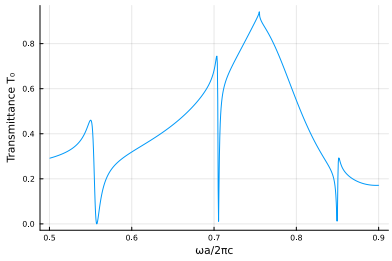

FIG. 10: Second example. Transmittance as a function of normalized angular frequency, for a normalized Bloch wavenumber of 0.25, as marked with a dashed line in Fig. 9b.

C. Third example

We consider again the second grating of Fig. 8 with a variable sinusoidal amplitude of $A \times 0.4L/\pi$. For normal incidence ($\alpha_0 = 0$) we plotted the transmission efficiency

of the zeroth-order as a function of angular frequency ω, for three values of the amplitude A: 0, 0.01 and 0.1. This is shown in Fig. 11. As expected, for $A = 0$ the transmittance spectrum follows a typical Fabry–Pérot spectrum. However, for $A > 0$ we have that a previously guided mode becomes leaky and couples with external radiation, giving rise to a typical Fano lineshape around $\omega L/2\pi c \approx 0.995$, whose width increases as we increase the amplitude A.

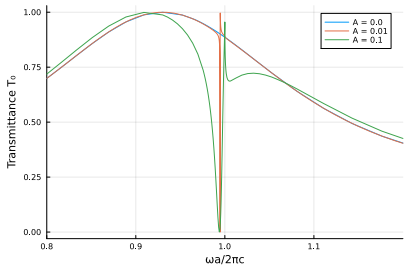

(a) Normalized angular frequency between 0.8 and 0.2.

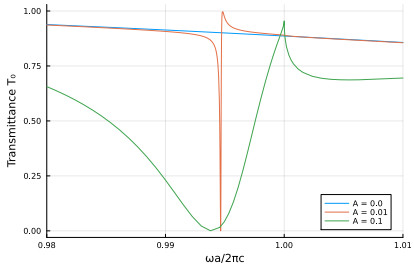

(b) Normalized angular frequency between 0.98 and 1.01.

FIG. 11: Third example. Transmittance of the zeroth-order diffraction as a function of normalized angular frequency, for various values of the sinusoidal amplitude A. A Fano lineshape is clearly distinguishable.

D. Fourth example

We consider again the second grating of Fig. 8 with a variable sinusoidal amplitude of $A\times 0.4L/\pi$, but this time adding a second harmonic to the profile, with amplitude $B\times 0.4L/\pi$ and phase $\phi = \pi/15$, which, for $B > 0$, breaks the mirror symmetry with respect to the yz plane. In Fig. 12, for normal incidence light ($\alpha_0 = 0$), we plot the transmission efficiency of the zeroth-order as a function of angular frequency ω, for various values of A and B. As expected, for $A = 0$ the transmittance spectrum follows a typical Fabry–Pérot spectrum, whereas for $A > 0$ a Fano lineshape emerges at $\omega L/2\pi c \approx 0.995$. What it is interesting is that for $A > 0$ and $B > 0$ a second Fano lineshape emerges at $\omega L/2\pi c \approx 0.772$. We hypothesize that, at $B = 0$, a Bound State in the Continuum (BiC) [19] is found around $\omega L/2\pi c \approx 0.772$. This is a guided mode, which is present in the radiative spectrum, but does not couple to it, it thus remains guided and does not turn leaky. The guided mode does not leak because of symmetry: it is odd with respect to the yz plane mirror symmetry, whereas the incident plane wave is even, and thus this mode cannot be excited. This corresponds to a *symmetry protected* BiC. The situation changes when $B > 0$, since the symmetry of the structure is now broken and the previously BiC becomes leaky and couples to the incoming wave, generating a Fano lineshape. In Fig. 12b it can be observed that a small Fano lineshape is also present at $\omega L/2\pi c \approx 0.772$ when $B = 0$. We believe that this is originated due to round-off errors, which render the structure slightly asymmetrical, even for $B = 0$.

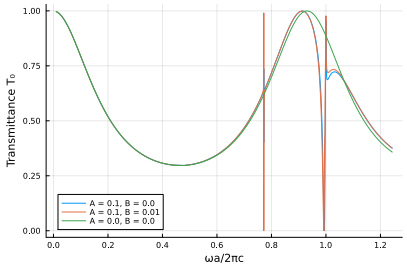

(a) Normalized angular frequency between 0 and 1.2.

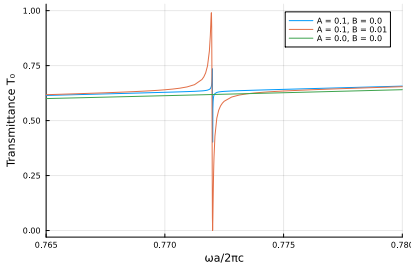

(b) Normalized angular frequency between 0.765 and 0.780.

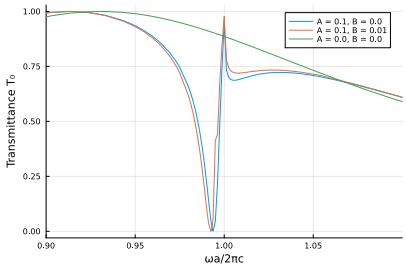

(c) Normalized angular frequency between 0.9 and 1.1.

FIG. 12: Third example. Transmittance of the zeroth-order diffraction as a function of normalized angular frequency, for various values of the sinusoidal amplitudes A and B.

E. Fifth example

We consider a photonic crystal (PhC) slab consisting in 16 layers of infinite cylinders, separated by a distance of L, with a radius of 0.2, and permittivity $\epsilon = 8.9$, as

depicted in Fig. 13. If the PhC slab extended indefinitely towards the negative y-direction, then it would have a projected band diagram, which is shown in Fig. 14, where a bandgap (in yellow) is found approximately between the normalized frequencies 0.28 and 0.45. For our finite PhC slab, we plotted in Fig. 15 the transmittance as a function of frequency, for normally incident light. The bandgap, where the transmittance drops abruptly to zero, is clearly seen around the normalized frequencies previously mentioned.

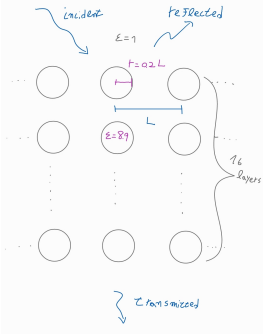

FIG. 13: Fifth example. PhC slab comprising 16 layers of infinite cylinders of permittivity 8.9, separation L and radius $0.2L$.

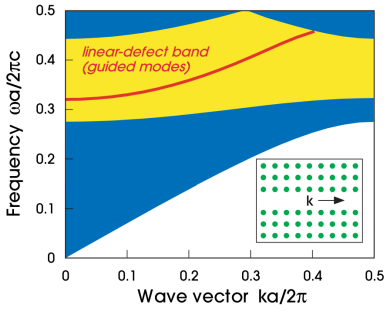

FIG. 14: Fifth example. Projected band diagram of the PhC shown in Fig. 13, if it had an infinite extension in the y-direction. Obtained from [20].

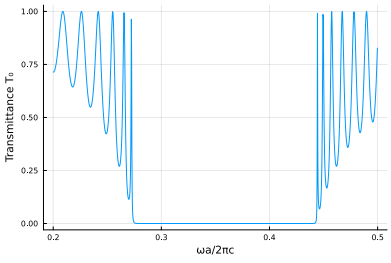

FIG. 15: Fifth example. Transmittance as a function of normalized angular frequency. A bandgap is clearly visible.

F. Sixth example

For our last example we consider a single row of our PhC slab, shown in Fig. 16, and we plot the condition number of the system matrix as a function of α_0 (or equivalently as a function of the angle of incidence), for a fixed angular frequency of $\omega L/2\pi c = 1.25$. This is shown in Fig. 17, where we have marked with a dashed line a Wood anomaly (where a new diffraction order emerges) at $\alpha_0 L/2\pi = 0.25$. We first observe that the condition number of the system is high in all cases, being in the order of 10^6. The fact that the BIE-NtD method yields ill-conditioned matrices was recognized by Lu and Lu [21], who proposed slight modifications to improve the conditioning of the resulting system. On the other hand, it is observed that, at the Wood anomaly, the condition number increases but remains in the same order of magnitude, which suggests that the BIE-NtD method could be robust at Wood anomalies.

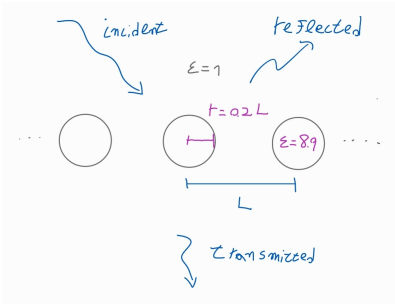

FIG. 16: Sixth example. A grating of a single row of cylinders.

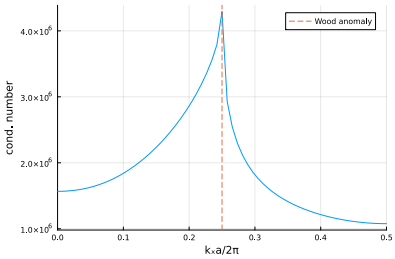

FIG. 17: Sixth example. Condition number of the resulting linear system as a function of the Bloch wavenumber (or angle of incidence), for a fixed normalized frequency of $\omega L/2\pi c = 1.25$.

V. CONCLUSION

In this report we have explained the operation of the BIE-NtD method, proposed by Wu and Lu [9] for the computation of transmission and reflection coefficients of 1D-periodic diffraction gratings and PhC slabs. Additionally, we established an analogy of this method with

the Transfer Matrix Method (TMM) for planar isotropic layered media, and recognized the BIE-NtD method as a direct generalization of the TMM for isotropic layered media with periodic interfaces. Finally, we have displayed various examples of interest employing the BIE-NtD method.

The BIE-NtD method, in its present state, is not efficient: it requires dense linear algebra operations, such as computing Schur complements, to solve the diffraction problem; this renders the overall methodology as slow and inapplicable for large and complicated settings. We believe that modifications could greatly improve the speed of the BIE-NtD. For example, we could avoid the use of Schur complements. This would increase the size of the resulting linear system, but it could be alleviated with the use of fast matrix-vector products schemes, such as the Fast Multiple Method [22], coupled with Krylov space iterative linear algebra solver, such as GMRES [23]. Alternatively, well-formulated Domain Decomposition methods can also be employed. On the other hand, we checked that the BIE-NtD method yields ill-conditioned system matrices. This issue is corrected in the next iteration of the method, presented in [21].

[1] Y. Wu and Y. Y. Lu, Boundary integral equation neumann-to-dirichlet map method for gratings in conical diffraction, JOSA A **28**, 1191 (2011).

[2] C. Linton, The green's function for the two-dimensional helmholtz equation in periodic domains, Journal of Engineering Mathematics **33**, 377 (1998).

[3] J. A. Monro Jr, *A super-algebraically convergent, windowing-based approach to the evaluation of scattering from periodic rough surfaces* (California Institute of Technology, 2008).

[4] O. P. Bruno, S. P. Shipman, C. Turc, and S. Venakides, Superalgebraically convergent smoothly windowed lattice sums for doubly periodic green functions in three-dimensional space, Proceedings of the Royal Society A: Mathematical, Physical and Engineering Sciences **472**, 20160255 (2016).

[5] A. Barnett and L. Greengard, A new integral representation for quasi-periodic scattering problems in two dimensions, BIT Numerical mathematics **51**, 67 (2011).

[6] A. Gillman and A. Barnett, A fast direct solver for quasi-periodic scattering problems, Journal of Computational Physics **248**, 309 (2013).

[7] T. Strauszer-Caussade, L. M. Faria, A. Fernandez-Lado, and C. Pérez-Arancibia, Windowed green function method for wave scattering by periodic arrays of 2d obstacles, Studies in Applied Mathematics **150**, 277 (2023).

[8] O. P. Bruno, M. Lyon, C. Pérez-Arancibia, and C. Turc, Windowed green function method for layered-media scattering, SIAM Journal on Applied Mathematics **76**, 1871 (2016).

[9] Y. Wu and Y. Y. Lu, Analyzing diffraction gratings by a boundary integral equation neumann-to-dirichlet map method, JOSA A **26**, 2444 (2009).

[10] M. Born and E. Wolf, *Principles of optics: electromagnetic theory of propagation, interference and diffraction of light* (Elsevier, 2013).

[11] O. Heavens, Optical properties of thin films, Reports on Progress in Physics **23**, 1 (1960).

[12] D. Colton and R. Kress, *Integral equation methods in scattering theory* (SIAM, 2013).

[13] E. Martensen, Über eine Methode zum räumlichen Neumannschen Problem mit einer Anwendung für torusartige Berandungen, Acta Mathematica **109**, 75 (1963).

[14] R. Kußmaul, Ein numerisches verfahren zur lösung des neumannschen außenraumproblems für die helmholtzsche schwingungsgleichung, Computing **4**, 246 (1969).

[15] D. L. Colton and R. Kress, *Inverse acoustic and electromagnetic scattering theory*, Vol. 93 (Springer, 1998).

[16] L. Li, Multilayer modal method for diffraction gratings of arbitrary profile, depth, and permittivity, JOSA A **10**, 2581 (1993).

[17] T. Magath and A. E. Serebryannikov, Fast iterative, coupled-integral-equation technique for inhomogeneous profiled and periodic slabs, JOSA A **22**, 2405 (2005).

[18] S. Fan, W. Suh, and J. D. Joannopoulos, Temporal coupled-mode theory for the fano resonance in optical resonators, JOSA A **20**, 569 (2003).

[19] C. W. Hsu, B. Zhen, A. D. Stone, J. D. Joannopoulos, and M. Soljačić, Bound states in the continuum, Nature Reviews Materials **1**, 1 (2016).

[20] J. D. Joannopoulos, S. G. Johnson, J. N. Winn, and R. D. Meade, Molding the flow of light, Princet. Univ. Press. Princeton, NJ [ua] (2008).

[21] W. Lu and Y. Y. Lu, High order integral equation method for diffraction gratings, JOSA A **29**, 734 (2012).

[22] L. Greengard and V. Rokhlin, A fast algorithm for particle simulations, Journal of computational physics **73**, 325 (1987).

[23] Y. Saad and M. H. Schultz, Gmres: A generalized minimal residual algorithm for solving nonsymmetric linear systems, SIAM Journal on scientific and statistical computing **7**, 856 (1986).